Noise-Activated And Noise-Induced Rhythms In Neural Systems

E. Mosekilde[1], O.V. Sosnovtseva[1], D. Postnov[2],
H.A. Braun[3], and M.T. Huber[3]

[1] Department of Physics,
The Technical University of Denmark,
2800 Kgs. Lyngby, Denmark

[2] Physics Department,
Saratov State University,
Astrakhanskaya Str. 83, Saratov, 410026, Russia

[3]Institute of Physiology,
University of Marburg,
Deutschhausstr. 2, D-35037 Marburg, Germany

Abstract The dynamical features of spike train generation in the presence of noise are investigated for three different models of neural rhythm generators: a single neuron model that simulates impulse pattern modulation for temperature encoding in mammalian cold receptors, a minimal neural network that describes transitions between beta and gamma rhythms in the brain and an electronic switching device that represents a simple breathing rhythm generator for a snail. We show that noise can explain a number of peculiarities in the observed spike trains, cause coherent switchings between different states, and induce new rhythms in small neural ensembles.

1 Introduction

The spatiotemporal characteristics of neural firing patterns in connection with brain function have received considerable interest, and many studies have been performed in order to understand the origin and role of various forms of synchronized neural activity (e.g., [1, 2]). Even single functional units demonstrate flexible neuronal patterns, and experimental recordings of peripheral sensory receptors and central neurons show more or less continuous transitions between different types of oscillatory patterns as a function of physiologically relevant stimuli [3, 4]. In accordance with experimental observations on mammalian cold receptors, the

---

Huber/Braun model [5], for example, reproduces tonic activities or bursting discharges due to slow oscillation cycles each triggering a group of impulses during its suprathreshold phase. Moreover, there exist irregular patterns of apparently chaotic origin [6, 7] while other patterns that can be explained only with essential contributions of noise are typical for thermosensitive neurons [4].

The complex and multifarious effects of noise on neural firing have not yet been fully understood. Neural activity is known to be noisy [8], and this stochastic feature is observed during both information transmission and spontaneous firing. At the same time, noise can play a constructive role in neural systems. In the presence of a subthreshold signal, the excitation threshold may be crossed when noise is superimposed onto the signal. This happens with high probability when the signal has its maximum and, hence, allows the biological system to detect signals that without noise would remain subthreshold [9, 10], demonstrating the effect of stochastic resonance [11]. An excitable neuronal system can exhibit the related phenomenon of coherence resonance [12]. In this case, there is no underlying periodic signal, and the resonance phenomenon is controlled by the noise intensity and the time of relaxation. Stochastic synchronization phenomena, i.e., the synchronization of noise-activated or noise-induced rhythms, have been studied in electrosensitive cells of the paddlefish by Neiman *et al.* [13]. Different types of noisy phase-locked regimes were observed.

Many neural systems can perform oscillations in different modes. Hence, the interesting questions arise: How is the dynamics of neural firing with *multimode* behavior affected by noise, and under what conditions can noise activate new rhythms? In this paper we focus on the following aspects:

(i) How can the presence of noise interfere with the spike generating mechanisms and the subthreshold oscillations in peripheral pattern generators, and under what conditions can it completely change the spiking pattern? The intrinsic dynamics is characterized by oscillatory changes in the membrane potential that are below or close to the spike threshold. In this situation naturally occurring stochastic influences due to membrane or synaptic noise can be an essential component in signal encoding. The reason is that the noise actually determines whether a spike is triggered during an oscillatory cycle or not. Hence, mixed patterns typically result, consisting of random sequences of spike-triggering and subthreshold oscillations;

(ii) How is the switching process between coexisting rhythmic activities in the brain influenced by noise? Brain oscillations are normally divided into different types based mainly on their frequency. Rhythms in the beta $(12 - 30Hz)$ and the gamma $(30 - 80Hz)$ ranges are found in many parts of the nervous system and are associated with attention, perception and cognition. Recently Kopell *et al.* [14] demonstrated that a model including both inhibitory interneurons and excitatory pyramidal cells can produce beta as well as gamma oscillations that employ different dynamical mechanisms to synchronize. The beta mode is able to synchronize with long conduction delays corresponding to signals traveling over a significant distance in the brain. Similar distances can not be tolerated by the gamma rhythms that are used more for local communication. It has been noted in electroencephalogram signals that rhythms of different frequencies can be found simultaneously [15]. In this connection we describe noise-induced activities in

terms of regularized switching events;

(iii) How can noise control the appearance of additional time scales in small neuron ensembles? In contrast to previous studies we investigate *noise-induced* rather than noise-activated oscillatory modes, i.e., we focus on time scales that are produced and controlled by noise and that do not exist in the deterministic case. We provide experimental observation of such multimode behavior and investigate the conditions for generation and entrainment of the various modes.

2 Tuning cold-receptor discharges

2.1 The Huber/Braun model

Mammalian cold receptors are particularly interesting in connection with the present analysis, both because of the complicated impulse patterns that they generate and because of the clear influence of noise. The impulse patterns are generally characterized by regular and relatively frequent burst discharges at intermediate temperatures with irregular and less frequent bursting patterns occurring at lower temperatures and irregular single spike discharges observed at higher temperatures. The stationary frequency *vs.* temperature characteristic typically displays a maximum at intermediate temperatures $(25 - 30^oC)$. This lack of monotonicity implies that the temperature encoding must be associated with the firing pattern as such and not only with the average firing rate. The Huber/Braun model of mammalian cold receptor was described in detail in Refs [5, 16]. In brief, it consists of two interacting minimal sets of ionic conductances, each including simplified de - and repolarizing Hodgkin-Huxley-type currents with sigmoidal steady state activation kinetics. For simplicity, inactivation is neglected. The two sets operate at different voltage levels and time scales. High threshold, fast activating currents are for spike generation (marked by indices d and r); low threshold, slow activating currents generate subthreshold potential oscillations (indices sd and sr). Including a leakage current I_l and the applied current I_{appl}, the membrane potential V is given by:

$$c\dot{V} \quad = \quad -I_l - I_d - I_r - I_{sd} - I_{sr} - I_{appl}, \tag{1}$$

with c denoting the membrane capacitance. In our generalized approach we do not refer to specific ionic currents but to the de- and repolarizing components of the two subsystems, the spike generator and the subthreshold oscillator. I_d is the fast depolarizing current and I_r is the fast repolarizing current which reflect the classical Na^+- and K^+-currents in the spike generation. The physiological basis for the two other currents, I_{sd} and I_{sr}, may be different in different neurons.

The leakage current is given by

$$I_l = g_l(V - E_l) \tag{2}$$

and the voltage-dependent ionic currents are expressed in the form:

$$
\begin{aligned}
I_i &= \rho g_i a_i (V - E_i), & (3) \\
a_{i\infty} &= 1/(1 + exp(s_i(V - V_{0i}))), & (4) \\
\dot{a}_i &= \phi(a_{i\infty} - a_i)/\tau_i. & (5)
\end{aligned}
$$

with $i = d, r, sd,$ and sr. Here, E_i are the equilibrium potentials, g_i the maximum conductances at the reference temperature T_0, and a_i the voltage and time-dependent activation parameters. ρ allows for the temperature scaling of the ionic currents. V_{0i} and s_i are half-activation potentials and slopes, respectively, of the steady state activation curves.

Exceptions to the above formulations are the assumed instantaneous activation of the fast depolarizing current

$$
a_d = a_{d\infty}, \tag{6}
$$

and the direct coupling of the slow repolarizing current to the slow depolarizing current:

$$
\dot{a} = \phi(\eta I_{sd} - k a_{sr})/\tau_{sr}. \tag{7}
$$

Here, η denotes the coupling constant and k is a relaxation factor.

The temperature dependences are expressed in terms of the scaling parameters ρ and ϕ for the maximum conductances and the time constants, respectively:

$$
\rho = 1.3^{(T-T_0)/\Delta}, \quad \phi = 3.0^{(T-T_0)/\Delta}. \tag{8}
$$

Here, T is the temperature at which the receptor cells operate, $T_0 = 25^o C$ is the reference temperature, and $\Delta = 10^o C$ is a scaling temperature. Each time T increases by Δ, the maximum conductance increases by a factor 1.3 and the time constants by a factor 3.

To account for the effect of random dynamics we have applied Gaussian white noise according to the Fox-Mueller algorithm [17]:

$$
g_w = (-4D \; h \; ln(a))^{1/2} cos2\pi b \tag{9}
$$

with a and b being random numbers between 0 and 1. h denotes the integration step, and the noise intensity is adjusted by the dimensionless parameter D. The noise is directly added to the membrane potential.

With the above simple temperature scaling and with noise implemented in the model equations, the full variety of experimentally observed impulse pattern evolves almost naturally. Increasing the temperature speeds up the ionic kinetics and leads to a faster dynamics of the subthreshold oscillator. This is associated with a decrease in the number of spikes that can be triggered per oscillation cycle.

2.2 Role of noise in pattern formation

Figure 1 reproduces some of the most characteristic patterns from experimental recordings for rat cold receptors [5] for direct comparison with the results of our modelling studies which are shown in the traces below. It can be seen that the model almost perfectly mimics all types of cold receptor discharges, but it also becomes evident that at least one type of pattern can be simulated only with the addition of noise. This is the pattern that consists of a mix of spike-generating and subthreshold oscillations (skippings) that typically occurs in the upper temperature range and can be seen in both experimental and modelling data (35°C, left diagrams) but not in the lowest diagram which is from a completely deterministic simulation (D=0). In this situation only the presence of noise allows the subthreshold oscillations to randomly exceed the threshold for spike-generation.
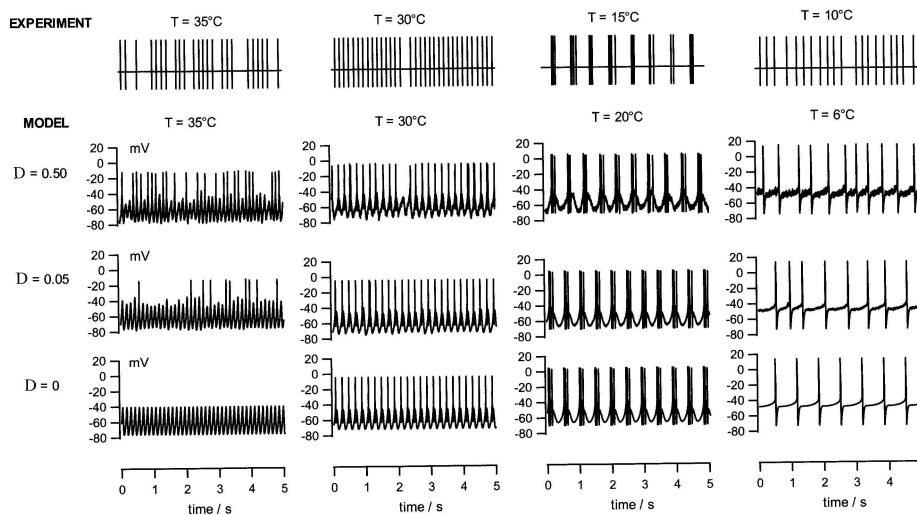

Figure 1: Typical impulse patterns for cold receptors at different temperatures. Comparison of experimentally recorded spike trains (upper traces) and modelling results from deterministic simulations ($D = 0$, lowest traces) and with addition of noise ($D = 0.05$ and $D = 0.5$, intermediate traces). The parameters of the numerical simulations are given in Ref. [18].

The second column shows the tonic firing patterns that typically can be seen in experimental recordings at normal skin temperatures around $30^{o}C$ and which also occur in our simulations with the appropriate temperature scaling. Noise does not seem to have major influence on the pattern generation. There is a regular tonic discharge because each oscillation cycle succeeds to trigger a spike – with a single exception: at $D = 0.5$ one of the oscillation cycles obviously fails to produce a spike. The upper trace indicates that a similar phenomenon may occur in the experimental recordings: a spike is missing within an otherwise regular tonic discharge. (Note that the simulation for $D = 0.5$ and $T = 30^{o}C$ has been

shifted along the time axis for the missing spike to occur at the same time as the spike in the experimental sequence). Although the missing spikes represent singular events, their occurrence suggests that noise cannot only induce spiking in otherwise completely subthreshold oscillations (as shown in the left traces) but can also prevent impulse generation in otherwise regularly spiking sequences. Such situations can cover a broad range of stimulus encodings.

In the third column of the figure we are comparing electrophysiological recordings and model simulations of different noise levels in the range of bursting discharges. More random input simply seems to induce more random fluctuations of spike-generation without any qualitative change of the pattern. This appears to also be the case at the lowest temperatures where the experimental recordings often exhibit irregular tonic discharges. The deterministic simulations generate completely regular discharges and the addition of noise is needed to produce the more realistically appearing irregular spike sequences.

With the addition of noise the model successfully reproduces the major types of experimentally recorded impulse patterns and it explains how these patterns can be related to the resonance behavior between slow subthreshold oscillations and spike generating mechanisms. The Huber/Braun model is valuable not only because it successfully simulates stationary cold receptor discharges, but also as a generalized neuronal pattern generator of significant flexibility.

3   Transitions between beta and gamma rhythms

3.1   The Kopell model

In a neural system, the individual neuron is generally located in an excitatory or inhibitory network that provides a variety of inputs to the neuron, primarily via the synaptic currents. In the present section we consider a minimal model for a neural network capable of producing both beta and gamma oscillations. Developed by Kopell *et al.* [14], the model includes two excitatory pyramidal neurons and one inhibitory interneuron. The network architecture is illustrated in Fig. 2 where open and filled arrowheads represent excitatory and inhibitory connections, respectively. Solid lines indicate fixed connections, and dotted lines represent connections that are varied during the simulations. By contrast to the single neuron considered in Sec. 2, the interesting features of the present system are connected with the interaction of the different neurons. Many factors contribute to making the environment of the network noisy. All of these factors are regarded as random external fluctuations. As we have seen in the previous section it is likely that neurons can use such external fluctuations to process their input signals more effectively. Here, we shall see how the presence of noise can generate transitions between different rhythmic modes in the network.

The Kopell model is based on Hodgkin–Huxley type neurons [19] which are modelled in accordance with the original formulation (rather than the simplified form used in the Huber/Braun model). There are no currents for subthreshold oscillations. Instead, there is an additional slow potassium current that accounts for after-hyperpolarization (ahp) in the excitatory neurons. The voltage of an excitatory neuron is controlled by the following differential equation:
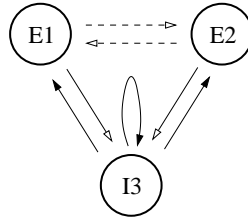
Figure 2: Architecture of the Kopell oscillatory network. E1 and E2 are excitatory cells, and I3 is an inhibitory cell. Open and filled arrowheads represent excitatory and inhibitory connections, respectively. Solid lines indicate fixed connections, and dotted lines represent synapses whose efficacies are varied in the simulations.

$$
\begin{aligned}
c\dot{V} =\ & -g_l(V - E_l) - g_{Na}m^3h(V - E_{Na}) - g_K n^4(V - E_K) \\
& -g_{ahp}w(V - E_K) - i^e_{syn} + i^e_{appl}.
\end{aligned} \tag{10}
$$

One recognizes the leak current $g_l(V - E_l)$, the sodium current $g_{Na}m^3h(V - E_{Na})$, the potassium current $g_K n^4(V - E_K)$, and the additional potassium current for after-hyperpolarization $g_{ahp}w(V - E_K)$. There is also a synaptic current input i^e_{syn} and a term for external current application i^e_{appl}. V is the membrane potential, E_j ($j = Na$ or K) is the Nernst (or reversal) potentials for the respective ions, and g_j the corresponding conductances. c is the membrane capacitance.

The gating variables are assumed to obey the standard dynamical equations:

$$
\begin{aligned}
\dot{m} &= \alpha_m(V)(1 - m) - \beta_m(V)m & (11) \\
\dot{h} &= \alpha_h(V)(1 - h) - \beta_h(V)h & (12) \\
\dot{n} &= \alpha_n(V)(1 - n) - \beta_n(V)n & (13) \\
\dot{w} &= \alpha_w(V)(1 - w) - \beta_w(V)w, & (14)
\end{aligned}
$$

where the α- and β-functions describe the voltage-dependent opening and closing rates for the various channels. For each excitatory neuron, a single equation controls the state of the synapses going from this neuron to others:

$$
\dot{s_e} = \alpha_{s_e}(V)(1 - s_e) - \beta_{s_e}s_e. \tag{15}
$$

Synaptic input to an excitatory neuron (here, E1) results in a current

$$
i^e_{syn,E1} = g_{ee}s_{e,E2}(V - E_e) + g_{ie}s_{i,I3}(V - E_i). \tag{16}
$$

In this expression, the s-variables refer to the presynaptic neurons (E2 and I3, respectively), whereas the voltage V refers to the postsynaptic neuron (E1). E_e and E_i denote the reversal potentials associated with excitatory and inhibitory synapses. A similar equation is used for the synaptic current of E2.

The inhibitory neuron I3 is very similar to E1 and E2, only the after hyperpolarization-current is not included:

$$
c\dot{V} = -g_l(V - E_l) - g_{Na}m^3h(V - E_{Na}) - g_K n^4(V - E_K) - i^i_{syn} + i^e_{appl} \tag{17}
$$

Noting that w does not appear, the remaining gating variables for the inhibitory neuron I3 are controlled by Eqs. (11–13).

Inhibitory synapses are governed by the equation:

$$\dot{s_i} = \alpha_{s_i}(V)(1 - s_i) - \beta_{s_i}s_i. \tag{18}$$

The inhibitory neuron receives inputs from E1 and E2 as well as from a mechanism of self-inhibition:

$$i^i_{syn,I3} = (g_{ei}s_{e,E1} + g_{ei}s_{e,E2})(V - E_e) + g_{ii}s_{i,I3}(V - E_i). \tag{19}$$

The detailed description of the various functions and parameter values can be found in the original paper [14]. Two parameters are varied in the present study: g_{ee}, the strength of the connections between E1 and E2, and g_{ahp}, the maximal conductance for the slow potassium ion channels.
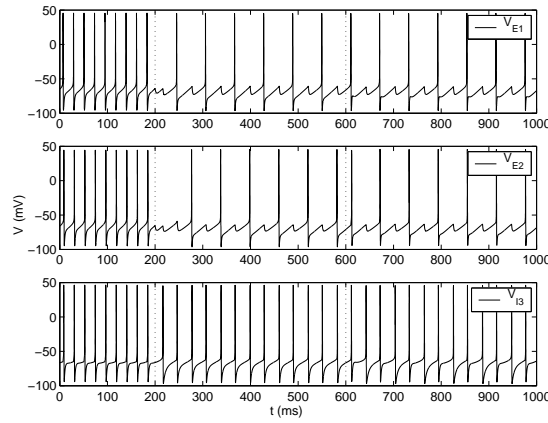

Figure 3: From top to bottom, the figures display the membrane potentials of the neurons E1, E2, and I3, respectively. For $t < 200 \ ms$, $g_{ee} = g_{ahp} = 0.0$ producing a gamma rhythm of about $45 - 50 \ Hz$. At $t = 200 \ ms$ a slowly varying potassium current is added by setting $g_{ahp} = 1.25 \ mS/cm^2$. This makes E1 and E2 switch to beta rhythms of $16 - 17 \ Hz$. Since the spikes of E1 and E2 are out of phase, the population of excitatory neurons considered as a whole still produces oscillations in the gamma band. Finally, at $t = 600 \ ms$ the E–E connections are added by setting $g_{ee} = 0.15 \ mS/cm^2$. This synchronizes E1 and E2, producing a beta rhythm in the E-population. For this plot, a transient of $100 \ ms$ was removed. From left to right, the modes observed here will be called γ, γ_{pop} and β.

As illustrated in Fig. 3, the Kopell model demonstrates three main network modes:

- For low values of the two parameters, the three neurons spike in synchrony with a frequency in the gamma band;

- If g_{ahp} is increased, the E1 and E2 neurons start to miss every other spike, lowering their individual frequencies into the beta band. However, since E1

and E2 are out of phase, the population of excitatory neurons as a whole
continues to produce gamma oscillations;

- Increasing the connection strengths between E1 and E2 makes the excitatory
  neurons spike simultaneously, thereby producing beta oscillations.

A scan over a two-dimensional parameter space was carried out for g_{ahp} varied
in the range $[0.0; 2.00 \ mS/cm^2]$ and g_{ee} varied in the range $[0.0; 0.30 \ mS/cm^2]$.
The initial conditions were identical for all calculations. To determine the spik-
ing mode, the regular spiking of I3 was used. First, the temporal location of the
I3 spikes was determined. Thereupon, a window of $\pm 5 \ ms$ around the I3 spikes
was searched for possible spikes in E1 and E2. For each point in the diagram,
spike trains for E1 and E2 were thereby produced. Hence, the oscillation mode
was characterized by these spike trains. A restriction was put upon this auto-
mated determination procedure, namely that the period of the oscillation mode
must be less than half the length of the spike train, thereby ensuring at least two
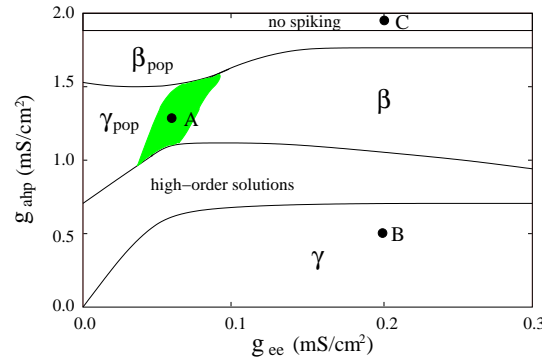occurrences of the full period.

Figure 4: Different oscillatory modes as functions of g_{ee} (the coupling between
excitatory neurons) and g_{ahp} (the conductance for the slow K-channel in excitatory
neurons). In the gray region, the γ_{pop}- and β-modes coexist. In the region denoted
high-order solutions we find a great variety of frequency-locked states.

The results are depicted in Fig. 4. Here, one can distinguish four to five differ-
ent oscillatory modes. For low values of g_{ahp}, the region denoted γ corresponds to
parameter values that generate gamma rhythms where all neurons (E1, E2, and
I3) spike in every cycle. The "gamma population" state γ_{pop} is located to the
left with intermediate values of g_{ahp}. In this region, the neurons E1 and E2 both
demonstrate beta rhythms of $16 - 17Hz$, but their overall behavior is found to
produce oscillations in the gamma band. There is a large region β occupied by
beta oscillations where E1 and E2 are in full synchrony with half the frequency of
the γ rhythm. With increasing g_{ahp}, they evolve into the beta population β_{pop}.
This state produces a beta rhythm, but only half as powerful as the beta state
described earlier since only one excitatory neuron (E1) spikes while another neu-
ron (E2) keeps silence. Within a range of parameters one can observe high-order

solutions with different combinations of spiking and silent states in the two excitatory neurons [21]. The dynamics seem to be limited in the g_{ahp}-direction by the appearance of a silent-state, in which E1 and E2 never spike due to the effects of the after-hyperpolarization current in combination with the spontaneous spiking of the I3 neuron. In the gray region, the γ_{pop}- and the β-modes coexist. The observation of a large region with coexisting solutions may have important inferences with respect to brain function. The question is: Can the Kopell model switch between the coexisting states? Physiologically, the externally applied current i_{appl}^e, together with ionic and synaptic currents, could represent the influence of other neurons of the brain. As previously noted, this influence may in many instances be considered as stochastic. Let us, therefore, examine the influence of fluctuations on the switching process.

3.2   Stochastic dynamics

Since noise may have different origins and can contribute in different ways, we assume that our network operate in a noisy field (Fig. 2). We represent this as Gaussian noise $\xi(t)$ with intensity D added to the first equations of each neuron.

Switchings between coexisting γ_{pop}- and β-modes

Let us choose the parameters to be in the region where γ_{pop} and β oscillations coexist (point A in Fig. 4). In the noiseless case, with the applied initial conditions, the resulting output oscillations is a β rhythm. This corresponds to a sharp peak in the power spectrum at $f_\beta = 17Hz$. With noise, an additional peak appears at $f_\gamma = 34Hz$. With increasing noise, the peak at f_β becomes broader and smaller in amplitude.

Aa a quantitative measure of coherence of switching events between two identified rhythms we use the so-called regularity coefficient which can be calculated as [12]:

$$R = <\tau> / \sqrt{<\tau^2> - <\tau>^2}, \qquad (20)$$

where τ is specified as the interspike interval. The time averaged duration identifies the mean period and, hence, the mean frequency $<f> = 1/<\tau>$ of the noise-activated oscillations.
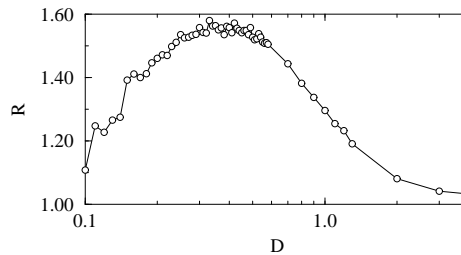

Figure 5: Regularity coefficient R calculated from the interspike intervals. ($g_{ahp} = 1.25\ mS/cm^2$, $g_{ee} = 0.05\ mS/cm^2$).

The spike train provides an efficient way to code a sequence of action potentials with nearly the same shape since the most important information in neuronal systems is widely believed to be coded in the time sequence of action potential generation [20]. The spike train is a binary time series with a value 1 at the time of action potential generations and 0 at other times. We analyzed the coherence properties for such binary spike trains in the presence of noise. The results of a calculation of the regularity coefficient (20) as a function of noise intensity are shown in Fig. 5. The curve is seen to display a maximum for noise intensities around $D = 0.4$. For weak noise, the contribution of γ_{pop} to the whole spike train is small. At the optimal noise intensity β and γ_{pop} contribute equally to the spiking train. Strong noise destroys the β rhythm, and the regularity decreases. This represents an example of coherence resonance in the noise-induced switching between different modes of the neural system.

Hopping between γ and β regimes

In the diagram presented in Fig. 4, regions of γ and β rhythms are separated by the region of high-periodic solutions. Fixing the parameters at the point B (Fig. 4), when adding noise we observe a *direct* transition between the main rhythms (Fig. 6).
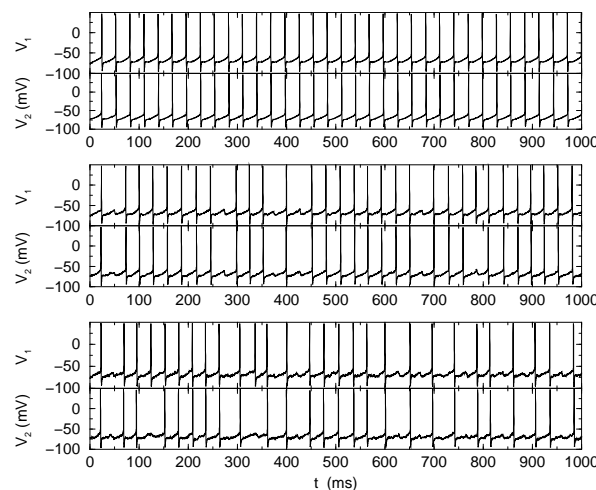

Figure 6: Switching process between γ and β rhythms for $g_{ahp} = 0.5 \ mS/cm^2$ and $g_{ee} = 0.2 \ mS/cm^2$. With increasing noise amplitude: $D = 0.2$ (top trace), 0.8 (middle trace), and 1.5 (bottom trace).

Figure 6 clearly shows how the residence time in the β regime now grows with increasing noise intensity. Our measure of coherence calculated over the interspike intervals indicates a well-pronounced maximum at some optimal noise intensity at which β and γ spike trains alternate in a regular way (Fig. 7). Here, we observe another example of regularized hopping events induced by applied noise, but now with one of the involved states being unstable for the considered parameters.
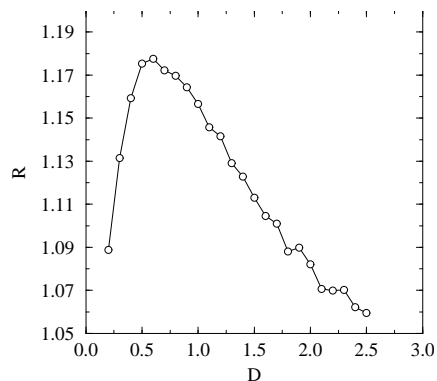
Onset of spiking dynamics

Figure 7: Coherence dynamics of interspike intervals in the Kopell model for $g_{ahp} = 0.5 \ mS/cm^2$ and $g_{ee} = 0.2 \ mS/cm^2$. As before, D represents the noise amplitude.

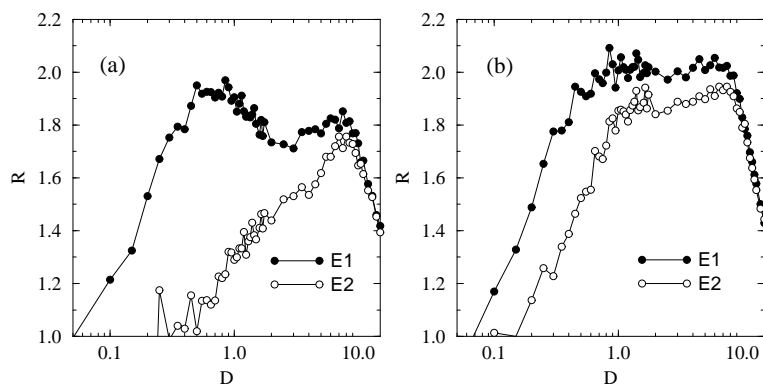Figure 8: Regularity for (a) $g_{ahp} = 2.0 \ mS/cm^2$, $g_{ee} = 0.0 \ mS/cm^2$ and (b) $g_{ahp} = 2.0 \ mS/cm^2$, $g_{ee} = 0.2 \ mS/cm^2$. Note, how the two peaks observed in (a) are closer to one another in (b).

Let us hereafter see how noise can cause firing events in this local network. (Parameter values corresponding to point C in Fig. 4). It is known that the behavior of spike trains can exhibit coherence resonance at an optimal noise intensity, as described for a single Hodgkin-Huxley model by Lee *et al.* [22]. In this case, noise affects the dynamics of the system in two ways: (i) Increasing the noise intensity decreases the activation time so that the contribution of the spiking dynamics increases. This enhances the regularization of spiking dynamics of the membrane potential. (ii) Noise also produces amplitude and phase fluctuations of the firing dynamics, destroying the periodicity in spiking events. The competition of these two mechanisms produces the phenomenon of coherence resonance, i.e. a maximal degree of coherence for an optimal noise level. This phenomenon is responsible for the first peak of coherence for E1 (Fig. 8). With vanishing connection between the excitatory cells ($g_{ee} = 0.0$), E2 demonstrates coherence of spiking events at a higher noise intensity because of its different internal parameters. Due to inhibitory synapses (controlled directly in the Kopell model by varying g_{ii} and g_{ie}), the first neuron adjusts its spiking behavior with respect to another neuron and demonstrates a secondary coherence resonance at higher noise intensity (Fig. 8a). When the E1–E2 connection is introduced ($g_{ee} = 0.2mS/cm^2$), the two peaks approach one another and the excitable units demonstrate a well-pronounced peak of coherence at the same noise intensity. This is illustrated in Fig. 8b. Because of the synchronization effects, the maximal value of R is higher than in the previous case [23].

4   Noise-induced rhythms

Let us hereafter focus on *noise-induced* rather than on noise-activated oscillatory modes. This implies that we focus on time scales that are generated and controlled by noise and do not exist in the deterministic case. We provide experimental observation of such multimode behavior and investigate the conditions of generation and entrainment of the specified modes.

The purpose of this section is to describe the two-mode stochastic behavior of an electronic system that has been constructed as a hard-wired version of the simplest breathing rhythm generator for a snail (Fig. 9) [24]. A single monovibrator circuit [25], being the functional unit in our electronic experiment, captures the essential aspects of excitable systems generating a single electric impulse whenever the input voltage exceeds the threshold level. The implementation of interacting excitable units shown in Fig. 10a contains self- and mutually inhibitory coupling chains that can increase the threshold voltages of the first (V_{th1}) and second (V_{th2}) units. Each coupling chain contains a rectifier and a low-pass filter with coupling strength g_{ij} and time constant τ_{ij}, where i, j denote the unit numbers. Note that the self-inhibitory time constants were chosen to be equal and to be greater than the mutually inhibitory time constants, i.e., $\tau_{11} = \tau_{22} > \tau_{12} = \tau_{21}$.

With a small noise intensity D (which is the same for the two units), both excitable units keep silent most of the time, and their threshold voltages remain equal ($V_{th1} \approx V_{th2}$). For intermediate noise levels, the coupling influence on the threshold voltages becomes significant. At the same time, since mutual inhibition makes the in-phase regime unstable, one of the two units gets the upper hand with
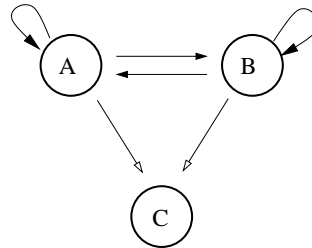
Figure 9: Schematic presentation of a breathing rhythm generator for a snail.
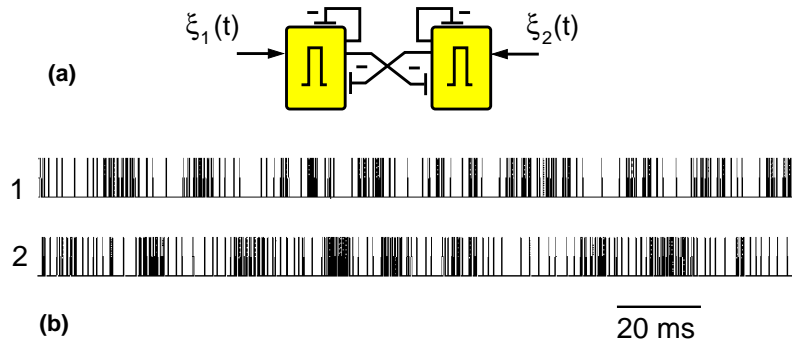

Figure 10: (a) Two monovibrators with delayed inhibitory couplings imitate the simple neural circuit. $\xi_{1,2}(t)$ represents external noise generator; (b) Stochastic spike trains generated by the first and second excitable units. Antiphase behavior is indicated on the average.

respect to its ability to suppress the firings of the other. However, with intensive firing, the slow self-inhibitory chain with rate τ_{11} (or τ_{22}) comes into operation and suppresses the activity of the stronger unit. This creates better conditions for excitation of the other unit, and the process continues in an alternating manner, producing a behavior with time-varying firing rates for the two excitable units (Fig. 10b).

In this operating regime, two peaks in the power spectrum are clearly distinguished (Fig. 11a). The high frequency peak corresponds to noise-induced oscillations in the single system while the low frequency peak reveals a new noise-induced oscillatory mode. Hence, the system of coupled excitable units generates a new oscillatory mode that is characterized by the values of τ_{ij} and by the relation between the noise intensity and the initial threshold voltages (V_{th1},V_{th2}). Figure 11b demonstrates how the frequencies of these oscillations (open circles) depend on the noise intensity. Inspection of the figure clearly shows that with increasing noise strength, both frequencies grow (i.e., they are noise-controlled), but the growth rates are different (i.e., they operate independently of each other). For strong noise, an excitable system can be immediately pushed out from the equilibrium state in spite of the threshold voltage. The low frequency peak in the power spectrum disappears, and the additional time scale no longer exists.
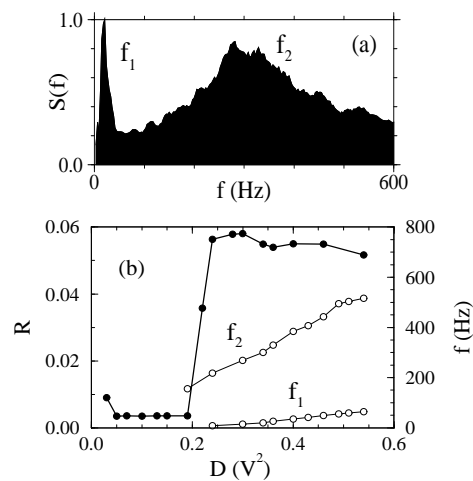

Figure 11: Two-mode dynamics in the excitable system presented in Fig. 10a. (a) Power spectrum with well-pronounced peaks ($D = 0.34V^2$) and (b) peak frequencies (open circles) and measure of regularity R (filled circles) *vs.* noise intensity D.

Figure 11b illustrates how the output regularity R (filled circles) is suddenly increased when low frequency oscillations appear while the peak at the noise-induced eigenfrequency f_2 becomes washed out because of the threshold modulation. Hence, arising due to interaction between excitable units, the low frequency oscillatory mode is controlled by noise via the effect of coherence resonance that brings ordering to the whole system.

5   Discussion

We considered noise-activated and noise-induced rhythms in models representing three different neural systems: (i) a single-neuron model of a peripheral pattern generator (a mammalian cold receptor), (ii) a small neural network (the Kopell model) that can account for the coexistence of beta and gamma rhythms in the brain, and (iii) a coupled monovibrator system that can serve as a model of a simple breathing rhythm generator. Our results indicate that the interaction between stochastic phenomena and complex deterministic dynamics may lead to a variety of different phenomena of importance for neural rhythm generation.

The single neuron model mimics the discharge pattern of peripheral cold receptors where impulse generation is determined by slow-wave oscillations which trigger one or more impulses during their depolarizing phases. This holds true for both deterministic and stochastic simulations with the exception that noise can induce spiking as well as skipping around the onset of period-one activity. In the regular bursting range noise does not produce any qualitative effects on the pattern but mainly smoothens the deterministically abrupt transitions. In the chaotic regime noise destroys the fine structure of the bifurcations. Thus, noise is assumed to play an essential role in sensory neurons: spike generation is clearly phase-locked to the underlying oscillations but noise determines the threshold crossings and hence the times at which spikes are generated. In addition to serving as cellular substates for synchronization in neuronal networks, subthreshold oscillations can also serve as cellular substates for a sensitive and differential neuromodulatory control based on the intrinsic oscillatory dynamics as optimized by naturally occurring noise sources. Further studies on subthreshold oscillating neurons should encompass the interesting neuromodulatory and encoding properties which arise from cooperative effects of oscillations with noise.

The neuronal network model also displays spiking patterns that are modified in an essential manner by the presence of noise. Especially in the area with coexisting solutions, noise causes the network to jump from one state to the other. There is a sharp transition between the oscillatory mode and a hopping state between the coexisting solutions, and this transition is controlled by the noise intensity. The output signal demonstrates quite "regular" switchings for a certain noise intensity. Moreover, noise can initiate switchings in the region where the main beta and gamma oscillations are separated by high-periodic solutions in the parameter space. In this case, we again observe an optimal noise intensity at which the jumping behavior becomes coherent. A particularly interesting finding is that, due to synaptic inhibitory interaction, the excitatory cells can demonstrate double coherence resonance [26]. With the introduction of a coupling between these neurons, the two peaks of regularity merge together, giving rise to further gain of regularity by virtue of synchronization.

We also showed that a simple system of coupled excitable functional units can generate a few oscillatory modes that are induced and controlled by noise [27]. Possible advantages of multimode dynamics may include: (i) Increased sensitivity via coherence resonance. We have found multiple coherence resonance phenomenon related to different frequency entrainments and to the appearance of additional time scales. (ii) Expanded flexibility. The presence and interaction of two distinct

oscillatory modes enrich the dynamical patterns. The electronic approach involving excitable stochastic units with self- and mutually inhibitory couplings can be applied to simulate neuron systems with *a priori* given phase relations.

6 Acknowledgments

References

[1] R. Eckhorn, R. Bauer, W. Jordan, M. Brosch, W. Kruse, W. Munk, and H.J. Reitboeck, Coherent oscillations: A mechanism of feature linking in the visual cortex?, Biol. Cybern. 60 (1988), 121-130.

[2] C.M. Gray, P. König, A.K. Engel, and W. Singer, Oscillatory responses in cat visual cortex exhibit inter-columnar synchronization which reflects global stimulus properties, Nature 338 (1989), 334-337.

[3] H.A. Braun, H. Bade, and H. Hensel, Static and dynamic discharge patterns of bursting cold fibers related to hypothetical receptor mechanisms, Pflügers Arch. 386 (1980), 1-9.

[4] H.A. Braun, K. Schäfer, H. Wissing, and H. Hensel, Periodic transduction processes in thermosensitive receptors, in, Sensory Receptor Mechanisms (eds. W. Hamann, A. Iggo), World Scientific, Singapore, (1984), 147-156.

[5] H.A. Braun, M.T. Huber, M. Dewald, K. Schäfer, and K. Voigt, Computer simulations of neuronal signal transduction: The role of nonlinear dynamics and noise, Int. J. Bifurcation Chaos 8 (1998), 881-889.

[6] W. Braun, B. Eckhardt, H.A. Braun, and M.T. Huber, Phase space structure of a thermoreceptor, Phys. Rev. E 62 (2000), 6352-6360.

[7] U. Feudel, A. Neiman, X. Pei, W. Wojtenek, H.A. Braun, and M.T. Huber, Homoclinic bifurcations in a Hodgkin-Huxley model of thermally sensitive neurons, Chaos 10 (2000), 231-239.

[8] H.C. Tuckwell, "Stochastic Processes in the Neurosciences", SIAM, Philadelphia, 1989; J.G. Taylor, Neurodynamics, (eds. F. Faseman and H.D. Doebner), World Scientific, Singapore (1991), 129-164.

[9] H.A. Braun, H. Wissing, K. Schäfer, and M.C. Hirsch, Oscillation and noise determine signal transduction in shark multimodal sensory cells, Nature 367 (1994), 270-273.

[10] D.F. Russell, L.A. Wilkens, and F. Moss, Use of behavioural stochastic resonance by paddle fish for feeding, Nature 402 (1999), 291-294.

[11] K. Nakamura, Stochastic Resonance in the FitzHugh-Nagumo Neuron Model, Proc. Inst. Natural Sci. 35 (2000), 179-185.

[12] A.S. Pikovsky and J. Kurth, Coherence resonance in a noise-driven excitable system, Phys. Rev. Lett. 78 (1997), 775-778.

[13] A. Neiman, X. Pei, D. Russell, W. Wojtenek, L. Wilkens, F. Moss, H.A. Braun, M.T. Huber, and K. Voigt, Synchronization of the noise electrosensitive cells in the paddlefish, Phys. Rev. Lett. 82 (1999), 660-663.

[14] N. Kopell, G.B. Ermentrout, M.A. Whittington, and R.D. Traub, Gamma rhythms and beta rhythms have different synchronization properties, Proc. Nat. Acad. Sci. USA 97 (2000), 1867-1872.

[15] S. L. Bressler, R. Coppola, and R. Nakamura, Episodic multiregional cortical coherence at multiple frequencies during visual task performance, Nature 366 (1993), 153-156.

[16] H.A. Braun, M.T. Huber, N. Anthes, K. Voigt, A. Neiman, X. Pei, and F. Moss, Interaction between slow and fast conductances in the Huber/Braun model of cold-receptor discharges, Neurocomputing 32-33 (2000), 51-59.

[17] R.F. Fox, I.R. Gatland, R. Roy, and G. Vemuri, Fast accurate algorithm for numerical simulation of exponentially correlated colored noise, Phys. Rev. A 38 (1988), 5938-5940.

[18] 1) Equilibrium potentials: $E_{sd} = E_d = 50$, $V_{sr} = V_r = -90$, $V_l = -60$ (mV); 2) ionic conductances: $g_l = 0.1$, $g_d = 1.5$, $g_r = 2.0$, $g_{sd} = 0.25$, $g_{sr} = 0.4$ (mS/cm^2); 3) membrane capacitance: $C = 1$ $(\mu F/cm^2)$ gives a passive time constant $\tau_M = C/g_l = 10$ (ms); 4) activation time constants: $\tau_r = 2$, $\tau_{sd} = 2$, $\tau_{sr} = 2$ (ms); 5) slope of steady state activation: $s_d = s_r = 0.25$, $s_{sd} = 0.09$; 6) half activation potentials: $V_{0d} = V_{0r} = -25$, $V_{0ds} = -40$ (mV); 7) coupling and relaxation constants for I_{sr}: $\eta = 0.012$, $k = 0.17$; 8) reference temperature: $T_0 = 25$ (^oC).

[19] A.L. Hodgkin and A.F. Huxley, A quantitative description of membrane current and its application to conduction and excitation in nerve, J. Physiol. 117 (1952), 500-544.

[20] G.P. Moore, D.H. Perkel, and J.P. Segundo, Statistical analysis and functional interpretation of neuronal spike data, Ann. Rev. Physiol. 28 (1966), 493-522.

[21] A. Fausbøll, "Analysis of a Minimal Network of Cortical Neurons" , MSc. Thesis, DTU, Denmark, 2001.

[22] S.-G. Lee, A. Neiman, and S. Kim, Coherence resonance in a Hodgkin-Huxley neuron, Phys. Rev. E 57 (1998), 3292-3297.

[23] D.E. Postnov, D.V. Setsinsky, and O.V. Sosnovtseva, Stochastic synchronization and the growth in regularity of the noise-induced oscillations, Tech. Phys. Lett. 27 (2001), 49-55.

[24] M.R. Rosenzweig, A.L. Leiman, S.M. Breedlove, "Biological Psychology", Sinaur Associated, Inc. Sunderland, Massachusetts, 1996.

[25] D.E. Postnov, S.K. Han, T. Yim, and O.V. Sosnovtseva, Experimental observation of coherence resonance in cascaded excitable systems, Phys. Rev. E 59 (1999), 3791-3794; S.K. Han, T. Yim, D.E. Postnov, and O.V. Sosnovtseva, Interacting coherence resonance oscillators, Phys. Rev. Lett. 83 (1999), 1771-1774.

[26] O.V. Sosnovtseva, D. Setsinsky, A. Fausbøll, E. Mosekilde, Transitions between beta and gamma rhythms in neural systems, Phys. Rev. E 66 (2002), 041901(6).

[27] D.E. Postnov, O.V. Sosnovtseva, S.K. Han, and W.S. Kim, Noise-induced multimode behavior in excitable systems, Phys. Rev. E 66 (2002), 016203(5).